Biomaterials 311 (2024) 122681

Contents lists available at ScienceDirect

Biomaterials

journal homepage: www.elsevier.com/locate/biomaterials

# Liver bioprinting within a novel support medium with functionalized spheroids, hepatic vein structures, and enhanced post-transplantation vascularization

Zhuoran Jiang [a,b,1], Bao Jin [a,1], Zhu Liang [d,e,1], Yinhan Wang [a,1], Shuai Ren [b], Yongfa Huang [a], Changcan Li [a], Hang Sun [a], Yunzhu Li [g], Li Liu [b], Nianlin Li [b], Jinzhuo Wang [b], Zhanfeng Cui [b,c], Pengyu Huang [f,**], Huayu Yang [a,***], Yilei Mao [a,*], Hua Ye [b,c,****]

[a] Department of Liver Surgery, Peking Union Medical College (PUMC) Hospital, PUMC & Chinese Academy of Medical Sciences (CAMS), Beijing, China
[b] Institute of Biomedical Engineering, Department of Engineering Science, University of Oxford, OX3 7DQ, UK
[c] The Oxford Suzhou Centre for Advanced Research (OSCAR), University of Oxford, Suzhou, 215123, China
[d] Target Discovery Institute, Centre for Medicines Discovery, Nuffield Department of Medicine, University of Oxford, Oxford, OX3 7FZ, UK
[e] Chinese Academy of Medical Sciences (CAMS), CAMS Oxford Institute (COI), Nuffield Department of Medicine, University of Oxford, Oxford, OX3 7FZ, UK
[f] Engineering Research Center of Pulmonary and Critical Care Technology and Device (MOE of China), Institute of Biomedical Engineering, Chinese Academy of Medical Sciences and Peking Union Medical College, Tianjin, 300192, China
[g] Department of Plastic and Reconstructive Surgery, Peking Union Medical College (PUMC) Hospital, PUMC & Chinese Academy of Medical Sciences (CAMS), Beijing, China

ARTICLE INFO

*Keywords:*
Primary hepatocytes
3D printing
Liver regeneration
Biocompatible hydrogel
Tissue engineering
Vascularized organs

ABSTRACT

Cell-laden bioprinting is a promising biofabrication strategy for regenerating bioactive transplants to address organ donor shortages. However, there has been little success in reproducing transplantable artificial organs with multiple distinctive cell types and physiologically relevant architecture. In this study, an omnidirectional printing embedded network (OPEN) is presented as a support medium for embedded 3D printing. The medium is state-of-the-art due to its one-step preparation, fast removal, and versatile ink compatibility. To test the feasibility of OPEN, exceptional primary mouse hepatocytes (PMHs) and endothelial cell line-C166, were used to print hepatospheroid-encapsulated-artificial livers (HEALs) with vein structures following predesigned anatomy-based printing paths in OPEN. PMHs self-organized into hepatocyte spheroids within the ink matrix, whereas the entire cross-linked structure remained intact for a minimum of ten days of cultivation. Cultivated HEALs maintained mature hepatic functions and marker gene expression at a higher level than conventional 2D and 3D conditions *in vitro*. HEALs with C166-laden vein structures promoted endogenous neovascularization *in vivo* compared with hepatospheroid-only liver prints within two weeks of transplantation. Collectively, the proposed platform enables the manufacture of bioactive tissues or organs resembling anatomical architecture, and has broad implications for liver function replacement in clinical applications.

* Corresponding authors. Department of Liver Surgery, Peking Union Medical College (PUMC) Hospital, PUMC & Chinese Academy of Medical Sciences (CAMS), No. 1 Shuaifuyuan, Wangfujing, Beijing 100730, China.
** Corresponding author.
*** Corresponding authors. Department of Liver Surgery, Peking Union Medical College (PUMC) Hospital, PUMC & Chinese Academy of Medical Sciences (CAMS), No. 1 Shuaifuyuan, Wangfujing, Beijing 100730, China.
**** Corresponding author. Institute of Biomedical Engineering, Department of Engineering Science, University of Oxford, OX3 7DQ, UK The Oxford Suzhou Centre for Advanced Research (OSCAR), Suzhou 215123, China.
*E-mail addresses:* huangpengyu@yeah.net (P. Huang), dolphinyahy@hotmail.com (H. Yang), pumch-liver@hotmail.com (Y. Mao), hua.ye@eng.ox.ac.uk (H. Ye).
[1] The authors contributed equally to the article.

https://doi.org/10.1016/j.biomaterials.2024.122681
Received 19 December 2023; Received in revised form 28 April 2024; Accepted 23 June 2024
Available online 25 June 2024

## 1. Introduction

Bioprinting aims to fabricate bioactive tissues or organs using specific living cells for treating diseases or testing modalities [1,2]. Extensive efforts have been made to engineer cell types, the cell-material niche, and the regeneration methodology [3]. However, direct printing of cell-laden bioink to rebuild both functional and structurally intact organs or tissues *in vitro* can be a challenge. Conventionally, extrusion-based bioprinting is employed, in which cell-laden bioinks are printed layer-by-layer [4,5]. This procedure inevitably restricts the print volume and cell numbers [6–8]. Bioink development efforts have sought to enhance the self-spanning ability of filaments for volume increments by modifying the chemical and rheological properties of the ink materials. Unfortunately, this approach generally compromises cell performance [9,10]. To overcome these limitations, embedded printing, which involves 3D printing within a support medium that counteracts

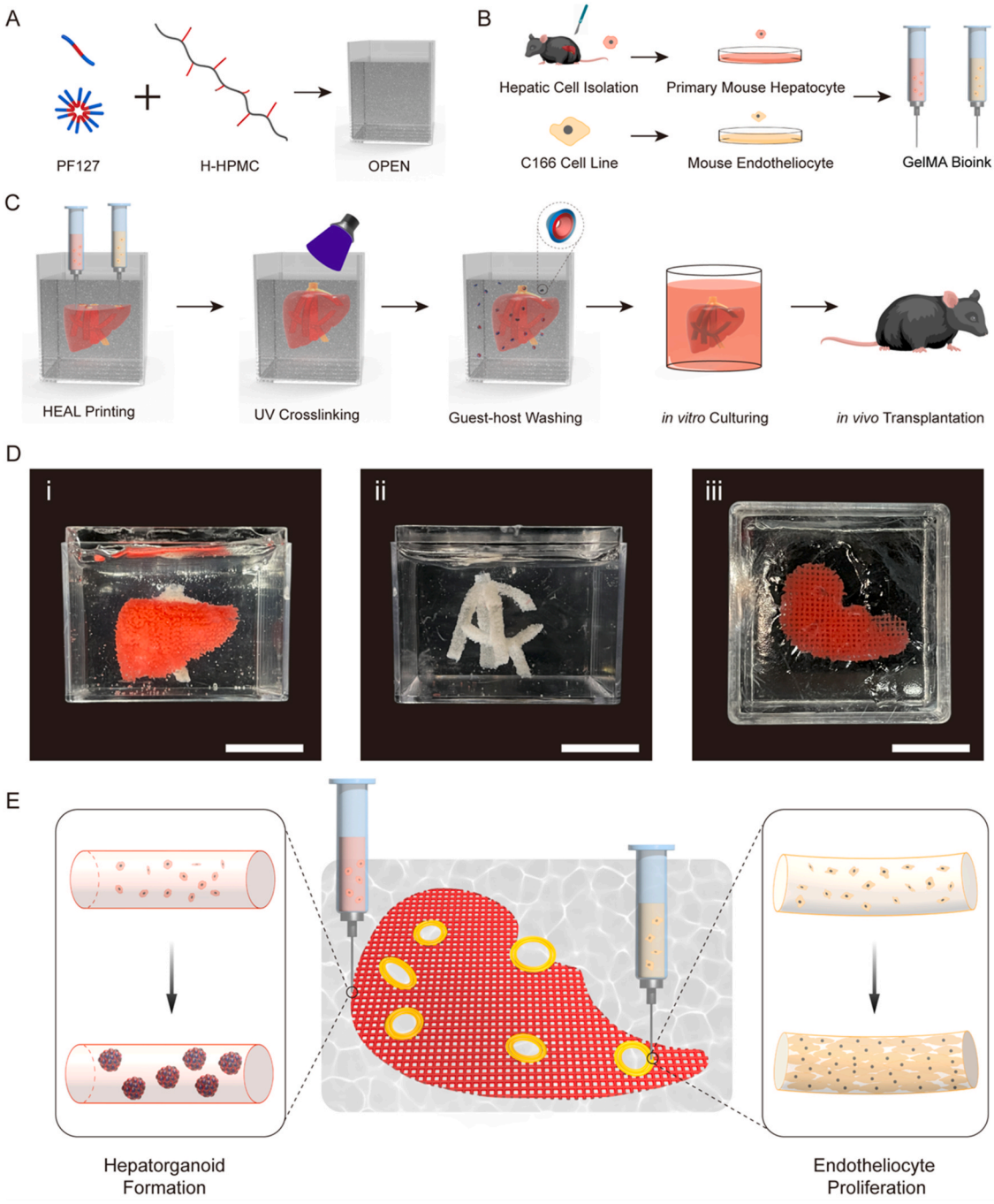


**Fig. 1. Transplantable and bioactive mini-liver via embedded 3D printing.** (A) Schematic illustration of the one-step OPEN preparation utilizing hydrophobic association between Pluronic® F-127 (PF127) and hydrophobically modified hydroxypropylmethyl cellulose (H-HPMC). (B) Isolation of PMHs, and 2D proliferation and the paired bioink preparation of PMHs and C166. (C) Step-by-step representation of the bioactive mini-liver regeneration process from heterogeneous embedded bioprinting *in vitro* to transplantation *in vivo*. (D) Images of printed constructs, stained by red or ivory dye. (i) Front view of HEAL, containing a latticed mini-liver and cylindrical veins. (ii) Front view of the vein system, including the portal veins and the hepatic veins. (iii) Top view of a printing layer from HEAL without vein. Scale bar, 20 mm. (E) A schematic diagram of HEAL printing within OPEN. The PMHs and C166 were then differentiated into matured hepatic spheroids and confluent endothelial cells.

gravitational force and surface tension, has been applied to print tissues, soft robots, biosensors and medical devices [11–14]. This alternative method allows for the design and construction of fine and delicate structures similar to *in vivo* structures such as vasculature and cavitation. In addition to designing a top-down biofabrication method, specific cell sources must be properly selected in order to regenerate target tissues or organs.

Recent advances combining top-down embedded bioprinting with bottom-up cellular self-organization have led to the development of thick vascularized tissues. Vascularized heart tissue, is of specific interest due to its inherent vascular hierarchy [15,16]. Although these advances represent a considerable progress in organ printing, they have limited ability to simultaneously maintain cell function and reproduce tissue structures, both *in vitro* and *in vivo*, thereby restricting their potential as transplant alternatives. Additionally, hollow organs like the heart and intestine are easier to construct than parenchymal organs, such as the liver and kidney, because parenchymal organs perform full physiological functions that require appropriate cell resources, completed cell-extracellular matrix (ECM) integration, and vascularization [17]. For example, liver cell populations consist of parenchymal and non-parenchymal cells. Hepatocytes represent approximately 70 % of liver cells and perform the primary physiological functions of liver [18]. Due to the complexity of liver, most research in liver 3D printing has focused on acellular surgical model reconstruction for preoperative visualization [19]. Recently, our research group *Huang* et al. found that 3D self-assembled mini-livers, prolonged the survival rate in mouse models of liver failure [20]. This study advanced 3D liver tissue as a treatment option for liver diseases [21]. Other advanced work in our lab regarding liver-based cell 3D includes *in vitro* carcinoma models reconstruction [22–24].

In this study, we aimed to construct three-dimensional, functional, and transplantable hepatospheroid-encapsulated-artificial livers (HEALs) via embedded bioprinting using self-organizable hepatocyte building blocks. The embedded printing procedure includes two steps: ink is extruded within a support to form the design construct, after which the supporting medium is removed to retain the desired structure [14]. The removal step is usually difficult to perform without disrupting the print structure, especially when the prints possess delicate vasculature constructs [12,13,25,26]. To achieve complex organ printing, we developed a polymer network based on hydrophobic interactions as the support medium. The key features of our proposed support medium, called an omnidirectional printing embedded network (OPEN), include: simplicity of preparation, straightforward support removal, and compatibility with different bioinks, while maintaining supporting stability, precise printing ability, and biocompatibility [27](Fig. 1A). Gelatin-methacrylate (GelMA) was then combined with OPEN to create cell-laden prints for tissue reconstruction. We used primary mouse hepatocytes (PMHs) as the hepatic cell building block for liver function reconstruction, with an originated culture medium that could induce hepatic spheroid formation *in vitro* [20]. To create cell-laden vein structures and induce post-transplantational vascularization, a mouse endothelial cell line, C166, was encapsulated within the GelMA as a vein-bioink (Fig. 1B and C). The resulting printed liver is termed HEAL (Fig. 1D). The printing paths of each HEAL layer were predesigned based on segmental liver anatomy so that dual nozzle printing could accurately reconstruct liver segments and veins accordingly (Fig. 1E). We demonstrated functional hepatocyte spheroid formation with marker protein expression and hepatic function *in vitro*. In addition, gene expression of printed hepatospheroids exhibited better resemblance to freshly isolated PMHs than conventional hepatocyte cultures, implying a higher potential for using HEALs in orthotopic liver transplantation. We also demonstrated that HEALs were transplantable and could substantially induce endogenous neovascularization by recruiting endothelial cells and growth factors.

## 2. Materials and methods

### 2.1. Embedding network, washing agent, and ink preparation

To create OPEN, 12.5 wt% (weight percentage for all materials, unless otherwise noted) Pluronic® F-127 (PF127, Sigma-Aldrich) was dissolved in phosphate buffered saline (PBS) at 4 °C overnight until complete solubilization. 2.5 wt% hydrophobically modified hydroxypropylmethyl cellulose (H-HPMC) (Sangelose 90L, Daido Chemical Co.) was gradually added to liquid PF127 with vigorous stirring in an ice bath to avoid clogging. The mixture was loaded into 50 mL conical tubes and centrifuged at around 1000 rpm for 1 min to remove any air bubbles. The blend was carefully transferred to acrylic boxes as printing chambers. The alpha-cyclodextrin (a-CD) powder was solubilized in PBS with vigorous stirring as paired polymer removal material. For bioprinting within OPEN, 12.5 wt% PF127 solution and 5 wt% a-CD solution were sterilized through 0.22 μm filters prior to mixing or further usage. 2.5 wt% H-HPMC powder and acrylic boxes were Ultraviolet (UV) irradiated overnight. 12.5 wt% GelMA was prepared by adding sterile saline to lyophilized GelMA polymer (SunP Gel G1, SunP Biotech Co.) and placed in a 70 °C water bath until complete dissolution. The liquefied GelMA was sterilized through 0.22 μm filters before being dispensed in Eppendorf tubes for storage at 4 °C.

### 2.2. Rheology measurements

The rheological characterizations of OPEN were obtained on a rotational rheometer (Discovery HR-2, TA instruments) using a 50 μm gap and a parallel plate of 40 mm diameter. The samples were transferred onto the test plate and heated from 0 to 40 °C with a ramp of 2 °C/min for temperature sweeps to study storage and loss moduli behavior as a function of temperature. Steady shear rate sweeps were conducted to measure the viscosity and yield stress of the polymer network at varying shear rate ranging from 0.01 to 1000 $s^{-1}$. To measure the self-healing ability, step-strain measurements were performed. A high strain magnitude (200 %) was applied to samples for 30 s followed by applying a low strain magnitude (1 %) for the same amount of time repeatedly at 30 °C. The removal ability of the washing agent was evaluated by the viscosity drop with a-CD additive, following steady shear rate sweeps excepted ranging from 0.1 to 1000 $s^{-1}$.

### 2.3. Morphology characterization and pore size calculation

The surface morphology of OPEN was observed using scanning electron microscopy (SEM, SU-8010, Hitachi) and environmental scanning electron microscopy (ESEM, ProX, Phenom) in dehydrated status at 5 kV and hydrated status at 15 kV, respectively. The hydrogel was freeze-dried in a vacuum chamber overnight and sputter-coated with gold before SEM imaging. The SEM and ESEM images were used to determine the distribution of pore sizes of OPEN by image analysis software (ImageJ, NIH). Transmission electron microscopy (TEM) samples were prepared by depositing hydrogel on glow-discharged carbon-coated TEM grids. After complete drying under room conditions, the specimens were imaged by the TEM (JEM-1400 Plus, JEOL).

### 2.4. Isolation of primary mouse hepatocytes and cell culture

The isolation and subculture protocol of PMHs were reported [28]. Briefly, PMHs were isolated from C57BL/6 mice following a modified two-step collagenase perfusion method. Prewarmed liver perfusion medium (Gibco) was injected into the liver through a catheter in the inferior vena cava at a rate of 6–8 ml/min. The portal vein was immediately cut off after 2–3 ml of perfusion, whereas the total perfusion volume was controlled around 40 ml. Then, a prewarmed digestion medium containing 0.5 mg/ml collagenase type I (Sigma) was perfused at a similar rate for another 5 min. Air bubbles were avoided during the

liver perfusion. The perfused liver was stripped from the peritoneal cavity post digestion, cutted into pieces, and filtered through a 70 mm filter. Centrifugation was then performed to separate hepatocytes at 50g for 5 min, repeated 3 times. After removal of the supernatant, the cells were resuspended in RPMI 1640 medium (HyClone) with 10 % fetal bovine serum (FBS, Gibco), and the suspension were inoculated into dishes pre-coated with rat tail type 1 collagen (Gibco) at density around $2 \times 10^4/cm^2$. Unattached cells were aspirated after 6 h by replacing the medium with hepatocyte maturation medium as previously reported [20]. PMHs were subcultured in a 5 % $CO_2$ incubator at 37 °C with medium change every 48 h, and passaged every 5–7 days at 1:3 ratio. The endothelial cells, namely C166 (BeNa Culture Collection) and human umbilical vein endothelial cells (HUVECs) (BeNa Culture Collection), were cultured in high-glucose Dulbecco's Minimal Eagle Medium (DMEM, Gibco) supplemented with 10 % FBS (Gibco) and 1 % penicillin/streptomycin (Gibco) at 37 °C under 5 % $CO_2$, and passaged prior to reaching 90 % confluence with medium change every other day. All cells were harvested by 0.25 % trypsin (Invitrogen) for further applications.

Bioprinting and acellular printing of HEALs with veins within OPEN, the sequential washing process, and imaging of artificial livers.

3D models of HEALs were generated using 3DS MAX (Autodesk) following the Couinaud's liver segmentation by hepatic vein and portal vein. The digital HEAL models were further converted to STL file format by RepetierHost software. Hepatocytes were harvested with an initial concentration of $1 \times 10^8$ cells/ml, while the C166 cells were harvested with an initial concentration of $5 \times 10^7$ cells/ml. To bioprint cell-laden HEALs with veins, 12.5 % GelMA solution, 2.5 % LAP solution, and $1 \times 10^8$ cells/ml of hepatocytes suspension or $5 \times 10^7$ cells/ml of C166 suspension were mixed following 8:1:1 ratio at 37 °C, respectively. The final composition of printable bioink was 10 % GelMA, 0.25 % LAP, and $1 \times 10^7$ cells/ml of hepatocytes or $5 \times 10^6$ cells/ml of C166. In addition, to print acellular constructs, simply replacing the cell suspensions with PBS stained by different dyes to distinct hepatic and vessel components. Here, we chose a red painting dye to represent the bioprinted liver component, whereas an ivory dye for the hepatic and portal veins. The inks were then loaded into syringes with 24G needles, The 24G needle, with a diameter of 0.55 mm, is employed for its compatibility with the rheological properties of GelMA, taking into account the bioink's potential expansion post-extrusion. And the syringes loaded with inks cooled at 4 °C for 20 min until complete physical gelation. The syringes were mounted into the extruders on the 3D printer (BioMaker 2, SunP Biotech) with temperature set to 20 °C, while the sterile acrylic box filled with OPEN was firmly placed on the printing bed with temperature set to 30 °C. The accuracy of bioprinting process is ensured by the precision of the BioMaker2 printer and the inherent properties of the GelMA bioink. The BioMaker2's motor resolution is defined as the minimum step size it can execute, which is 5 μm, offering fine control over the positioning of the print head. Upon completion of the printing process, the box containing HEAL was UV irradiated for 30 s to crosslink the printed constructs. The crosslinked structure was carefully transferred into a 6 well plate filled with sterile 3 or 5 % a-CD solution. The structure was gently shaken by a tweezer to remove the surrounding embedded polymer. It was then transferred into a new 6 well plate and cultured at 37 °C under 5 % CO2 with mature hepatocyte culture medium changing every 48 h. To image the dyed acellular artificial livers or the vein system, the washed structures were loaded into acrylic boxes with 20 % PF127 solution in low temperature. The box was then heated up to 30 °C to solidify the transparent Pluronic solution supporting the embedded HEALs for visualization.

### 2.5. Cell viability assay

To assess the viability of hepatocytes within a printed HEALs composed of crosslinked GelMA strands, a fluorescent live/dead assay was conducted following manufacturer's instructions. A mixture of calcein-AM (1 μmol/L, Sigma) and propidium iodide (PI) (2 μmol/L, Sigma) was freshly made prior to staining. The 3D printed HEALs were gently washed with PBS three times, and immediately incubated with the calcein-AM/PI mixture for 15 min at room temperature, avoiding any light exposure. After incubation, they were gently washed again with PBS for at least three times prior to fluorescent image acquisition under a laser scanning confocal microscope (C2/C2si, Nikon). The number of living and dead cells were calculated from independent field images from at least 6 biological replicates by ImageJ. Hepatocyte viability was assessed at day 1, 4, 7, 10, 14 and 21 post printing. To evaluate the biocompatibility of OPEN, HUVECs were harvested at $1 \times 10^6$ cells/ml, seeded on top of the polymer mixture, and cultured for 24 h. The live/dead staining process followed the aforementioned assay determining viability at hour 0, 3, 6, 12 and 24 post inoculation.

### 2.6. Immunofluorescence staining

Samples were fixed in 4 % paraformaldehyde for 20 min at room temperature, gently washed with PBS three times, and permeabilized with 1:200 Triton X-100 (Sigma) for 30 min. They were then blocked by 3 % Bovine serum albumin (BSA, Sigma) for 60 min at room temperature and washed with PBS three times. Next, the samples were stained with the following primary antibody solution overnight at 4 °C: chicken anti-albumin (anti-ALB, Abcam), rabbit anti-glutathione S-transferase (anti-GST, Abcam), anti-alpha-1-antitrypsin (anti-AAT, H7, Santa Cruz), mouse anti-CD31 (Abcam), anti-E-Cadherin (BD), rabbit anti-cytochrome P450 2E1 (anti-CYP2E1, Sigma), anti-cytochrome P450 3A4 (anti-CYP3A4, Homology to CYP3A11, Santa Cruz) and rabbit anti-multidrug resistance protein 2 (anti-MRP2, Abcam). All samples were rewarmed at room temperature for 30 min prior to primary antibody removal. The samples were washed with PBS three times and incubated with the following secondary antibody solution for 60 min at room temperature and protected from light: goat anti-mouse IgG Alexa Fluor 488 (Abcam), goat anti-rabbit IgG Alexa Fluor 488 (Abcam), goat anti-mouse IgG Alexa Fluor 594 (Abcam), goat anti-rabbit IgG Alexa Fluor 594 (Abcam), and goat anti-chicken IgG Alexa Fluor 594 (Abcam). The samples were washed 3 times followed by applying DAPI (Sigma) solution for 5 min or phalloidin conjugated to Alexa Fluor 488 (Servicebio) at room temperature depending on purpose. Sample observations were done by a laser scanning confocal microscope (C2/C2si Nikon) and photographed.

### 2.7. DiL-ac-LDL staining, periodic acid-schiff staining, and indocyanine green uptake and release assay

The hepatocyte laden samples were stained by dil-labeled acetylated low-density lipoprotein (DiI-ac-LDL, Invitrogen) following manufacturer's instructions. For the periodic acid-Schiff (PAS, Sigma) staining and indocyanine green (ICG, Sigma) uptake experiments, samples were first lysed by GelMA Lysate (SunP Biotech) at 37 °C on a rotary shaker following manufacturer's instruction. The mixture solution was filtered through 70 μm filters and centrifuged to collect hepatocytes for next steps. The isolated cells were stained with periodic acid-Schiff as per the manufacturer's instructions. As for the indocyanine green (ICG, Sigma) uptake experiments, the mature hepatocytes were incubated in the medium supplemented with ICG (1 mg/ml) at 37 °C for 60 min, and then washed with PBS three times to observe the update of ICG by microscope. The dyed cells were again incubated at 37 °C for 6 h, and washed 3 times with PBS to obtain ICG release from hepatocytes by microscope.

### 2.8. RNA extraction and quantitative real-time polymerase chain reaction (qPCR)

The printed samples were lysed by GelMA lysate at 37 °C on a rotary shaker for 45 min. The hepatocytes were collected by centrifugation after being filtered through 70 m filters to remove bioink residues. Three

different samples were used in each group. Total RNA was isolated from cells with the Trizol (Invitrogen) according to the manufacturer's instructions. 1 μg of RNA was reverse transcribed using a ReverTra Ace qPCR RT Master Mix with gDNA Remover Kit (Toyobo) in a 20 μl reaction. The qPCR was performed using the TransStart Tip Green qPCR SuperMix (TransGen Biotech) according to the manufacturer's instructions. The Delta-Ct method was used to calculate the relative RNA expression levels. The sequences of the primers used are given in the Primer Table in Supporting Table 1.

### 2.9. mRNA sequencing and analysis

The mRNA-seq analysis was carried out at Allwegene Technology Inc. (Beijing, China). The length of the RNA fragments was measured using the Agilent 2100 Bioanalyzer Instruments (Agilent, USA). The cDNA library was subsequently constructed using PCR amplification. RNA-seq using the PE150 sequencing method was carried out on the Illumina second-generation high-throughput sequencing platform. Then, adapters or reads with poor quality were filtered out. The alignment of transcriptomes and the analysis of transcript splicing were carried out separately on clean reads data using the Star and Cufflinks software (Ghosh and Chan, 2016). HTSeq software (Princeton University, USA) was used to examine the gene expression levels of each sample, using the union counting model. The gene expression was determined using a cutoff value of FPKM $>1$.

### 2.10. 3D printed body transplantation and neovascularization experiments

SPF-grade C57BL/6J male mice (6–8 weeks) were purchased from SiPeiFu Biotechnology Ltd. All animal procedures were performed in accordance with the National Institutes of Health guidance and were approved by the Committee and Institutional Review Board of the Peking Union Medical College and Hospital (No. XHDW-2023-076). For the *in vivo* transplantation, the HEALs were transplanted into the iliac fossa of the abdominal cavity. All procedures were performed under 1 % pentobarbital sodium anesthesia. All animals were maintained in pathogen free conditions at room temperature with free access to food and water.

Two weeks after transplantation of the 3D printed models into mice, 1 % fluorescein-dextran isothiocyanate (Sigma) was injected through the tail vein. The mice were then anesthetized and dissected to remove the neovascularized implants. The explanted printed tissues were either thoroughly washed with PBS for immunofluorescence staining as described above or fixed in 10 % formalin overnight prior to paraffin embedding for immunohistochemical staining. The quantitative angiogenesis analysis of implants was performed by AngioTool software (NIH) using a vessel thickness of 2 and a small particle filter of 20.

### 2.11. Histology and immunohistochemistry

Samples were fixed in 4 % paraformaldehyde and embedded in paraffin using standard procedures. Embedded specimens were cut into 5 μm thick paraffin sections following standard procedures. The sections were deparaffinized and dehydrated with xylene and anhydrous ethanol before immunohistochemical staining. They were then incubated in 3 % $H_2O_2$ and blocked for 20 min in 5 % goat serum. Next, they were stained with anti-CD31 (Invitrogen, 14-0311-82), anti-ALB (Invitrogen, MA5-32531), anti-AAT (Invitrogen, MA5-51077), anti-CYP2E1 (Invitrogen, MA5-32605) primary antibodies overnight at 4 °C. The next day, samples were incubated with the HRP-conjugated secondary antibody, followed by DAB staining. Dried and sealed slides were observed and imaged by microscope.

### 2.12. Statistical analysis

All data are shown as mean ± standard deviation. For most statistical assessments, the unpaired Student's t-test was applied in this study. Statistical analyses and plots were performed using GraphPad Prism 9. Differences were considered statistically significant if the p-value was less than 0.05. For all statistics, data from at least three independent samples or replicate experiments were used.

## 3. Results

### 3.1. Design and fabrication of the omnidirectional printing embedded network (OPEN)

There are two types of existing support medium: granular gel medium or bulk gel medium. Typical examples of the former are gelatin particles or Carbopol, which are limited by fabrication complications, working temperature window, and ionic sensitivity [11,12]. Bulk gel mediums, while easy to prepare, can be challenging to remove due to the difficulty in adjusting the medium's viscosity, which is necessary for the successful removal of the support medium from the construct [25,26]. In order to combine the ease of printing of a bulk gel medium with the ease of removal of a granular gel medium, we designed a supporting medium based on hydrophobic interactions [27]. This OPEN was formed by combining two FDA-approved and commercially available materials in a one-step mixing process. The materials used are H-HPMC and PF127 (Fig. 2A–i). Previous work showed that the Pluronic diblock copolymer alone is incompetent as a support material for free form writing, because the PF127 micelle entangled network is a non-recoverable hydrogel that can cause crevasse formation after nozzle movement [29]. Additionally, structures printed into PF127 suspensions sag due to PF127's liquid-dominated properties in the non-entangled micelle or unimer status. To overcome the limitations of PF127 alone, we hypothesized that the PF127 non-entangled micelle suspension can be leveraged with a hydrophobic polymer to form a supportive and recoverable network for omnidirectional 3D printing by physical crosslinking. To test this hypothesis, we selected biocompatible H-HPMC because the high density of hydrophobic moieties in low H-HPMC concentrations, promotes physical interactions between the hydrophobic core of PF127 micelles and the hydrophobic stearyl groups at the hydroxypropyl ends of H-HPMC (Fig. 2A–ii) [30,31]. After optimizing the component ratio of H-HPMC and PF127, we then determined that a-CD, also FDA approved, functions as an efficient removal agent. Application of a-CD to OPEN polymer networks promptly decreases network viscosity via a guest-host interaction between the hydrophobic inner cavity of a-CD (host) and the hydrophobic stearyl groups of H-HPMC (guest) [28,32]. Alone, the structure of a-CD resembles a hollow cone that is hydrophobic inside and hydrophilic outside. When H-HPMC is present, most of the side chains are encapsulated by the hydrophobic inner surface of a-CD, forming a rotaxane complex. This complex disrupts hydrophobic interactions among H-HPMC side chains, and hence the entire OPEN gel, causing the viscosity of OPEN decreasing [28,32] (Fig. 2A–iii).

We optimized OPEN's rheological properties to maximize its supporting ability by adjusting the weight percentages of Pluronic and H-HPMC. Temperature sweeps were performed on OPEN gels, starting from 15 wt% Pluronic, which is the maximum concentration before losing the non-entangled micelle structures, and 2.5 wt% H-HPMC, considering that the solubility limit of H-HPMC alone is around 3 wt% [33]. OPEN gels based on 12.5 wt% Pluronic exhibited stable solid properties and tunable moduli within the desired temperature window ranging from room temperature to body temperature which is suitable for bioprinting (Fig. 2B). Other compositions, such as 5 wt% and 10 wt% Pluronic, showed fluid-dominated properties, while 15 wt% Pluronic exhibited low moduli tunability (Supplementary Fig. 1A). We next characterized network formation in 12.5 wt% Pluronic-based OPEN gels by measuring gel yield stress and recoverability. As the H-HPMC

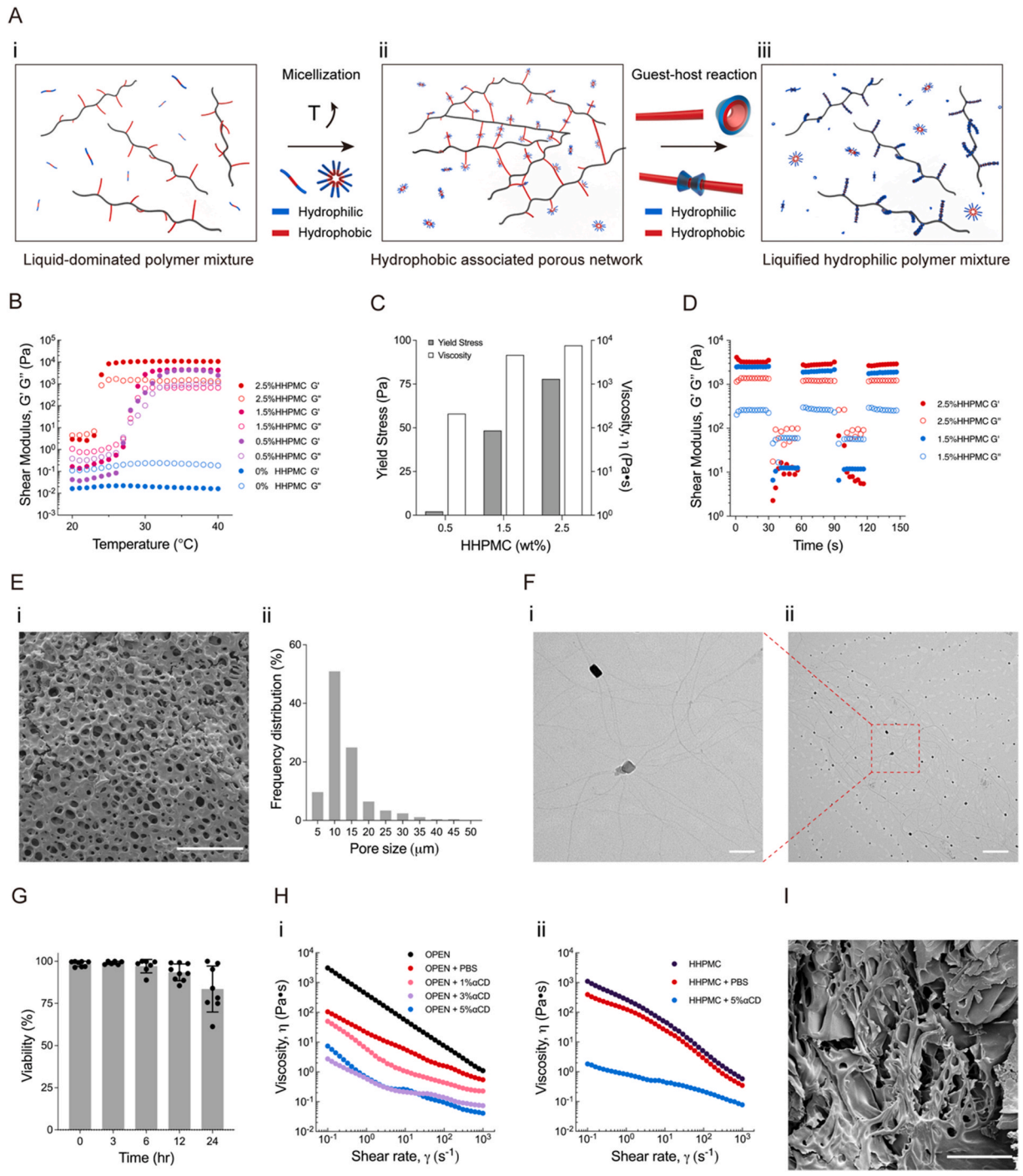


**Fig. 2. Systematic characterization of OPEN formation and liquification via rheology, morphology and compatibility evaluation.** (A) Schematic diagram of OPEN formation and thinning mechanisms. (i) The unimer PF127 and H-HPMC are homogeneously mixed to form liquid phase mixture at a temperature lower than the critical micellization temperature. (ii) The mixture is heated up to form the hydrophobic associated network for embedding printing. (iii) After printing, α-CD is utilized to change the network's hydrophobicity, leading to the liquification of polymer network. (B) Temperature sweep of mixture with 12.5 % PF127 and various H-HPMC concentration, indicating the temperature dependent sol-gel transition given by H-HPMC. (C) Desired yield stresses for printing (<100 Pa) are achieved by adding 1.5 or 2.5 % H-HPMC. (D) Step-strain measurements demonstrate the self-healing property of the polymer network. (E) SEM image of OPEN shows its porous network structure with average pore size lower than 20 μm. Scale bar, 100 μm. (F) TEM images of OPEN exhibit H-HPMC microfibrils associating around randomly distributed PF127 micelles. Scale bar, (i) 100 nm and (ii) 500 nm. (G) Biocompatibility of OPEN is assessed by a viability assay of cell-material direct contact within 24 h. A high cell survival rate is observed within 6 h n ≥ 6 for biological replicates. (H) (i) OPEN viscosity can be drastically decreased by adding 3-5 wt% α-CD. (ii) 5 wt% of α-CD drops the viscosity of H-HPMC similarly, confirming that H-HPMC plays a vital role in the proposed guest-host reaction. (I) SEM image of liquified OPEN, showing ruptured structure of the porous polymer network. Scale bar, 100 μm.

concentration increased (i.e. more hydrophobic moieties), higher yield stress and viscosity were observed, confirming a stronger hydrophobic association within the network [30,32]. Both 1.5 wt% and 2.5 wt% H-HPMC gels showed yield stress values under 100 Pa (Fig. 2C and Supplementary Fig. 1B). To investigate self-healing in OPEN gels, a high strain magnitude (200 %) was applied to disrupt network formation, followed immediately by regaining 1 % of strain (Fig. 2D). These two gel concentrations exhibited similar self-recovery properties within seconds. However, the network with the higher H-HPMC ratio demonstrated better storage modulus recovery over cycles of destruction and reformation. Therefore, we determined that 12.5 wt% Pluronic plus 2.5 wt% H-HPMC is the optimum composition for OPEN preparation based on its printing temperature window, supportive ability, and self-recovery. An evaluation of the network's supporting stability, printing precision, and compatibility with various crosslinking strategies is reported elsewhere [27].

Herein, we aim to explore the internal morphology of the gel network to elaborate its supporting mechanism. To probe the hydrophobic interactions associated with network formation, we examined the microscopic structure of OPEN. SEM images revealed that OPEN gels self-assemble into structures with near-uniformly distributed pores less than 20 μm in diameter on average (Fig. 2E and Supplementary Fig. 2A). However, OPEN gels made with a low concentration of either Pluronic or H-HPMC failed to assemble porous networks and demonstrated amorphous morphology (Supplementary Fig. 2B i-iii). Slightly reducing the concentration of H-HPMC to 1.5 wt% in a 12 wt% Pluronic based OPEN would give a heterogenous distribution of the pore sizes, which resulted in a lower yield stress and recovery ability compared to the optimum OPEN composition (Supplementary Fig. 2B iv). ESEM also confirmed that the majority of network pore sizes in its hydrated state are less than 20 μ m. (Supplementary Fig. 3A). The highly interconnected nature of H-HPMC fibers was also visualized (Supplementary Fig. 3B). In order to understand the formation and self-healing mechanism of OPEN, we have also looked into the multi-level molecular architecture of H-HPMC fibers through TEM [34,35]. The H-HPMC microfibrils exhibit flexible and high-aspect-ratio filaments in nanoscale (Supplementary Fig. 3C). The microstructure of PF127 micelles has been well investigated in the literature that they are highly homogenous spheres of approximately 20 nm in diameter [36,37]. As a hydrogel mixture of PF127 spherical micelles and H-HPMC fibrillar polymer, we hypothesized that the non-covalent interactions between the hydrophobic segments of PF127 micelles and the hydrophobic side chains of H-HPMC microfibrils regulated the self-assembling and shear-thinning properties [30,38]. The typical interactions between micelles and fibrils were shown in the TEM image that the H-HPMC microfibrils are assembled at randomly distributed PF127 micelles (Fig. 2F). During printing, the nozzle severed the porous OPEN gel as the shear stress caused by the nozzle exceeded the OPEN's yield stress. Meanwhile, bioink was deposited filling in crevasses. A rapid self-healing process took place after shear stress removal, due to the transient and reversible interactions between PF127 micelles and stearyl groups from H-HPMC [39–41]. Additionally, since OPEN is designed for bioprinting, we evaluated OPEN's biocompatibility through cell seeding. Cells remained viable (>97 %) for at least 6 h, which is longer than the printing process (Fig. 2G and Supplementary Fig. 4).

Furthermore, we observed efficient thinning behavior by 3-5 wt% a-CD additives (Fig. 2H and i), indicating that OPEN is easy to remove once printing is complete. Excessive dilution by solvent is often used as a common removal method for other support mediums, but does not effectively reduce the viscosity of OPEN. The drastic viscosity drop of OPEN constructs when a-CD is present, and not when more solvent is added, demonstrates that OPEN removal is specific, controlled, and only occurs via hydrophobicity inversion between H-HPMC and a-CD (Fig. 2H and ii). We verified a-CD's ability to destroy the porous OPEN gel and thereby cause OPEN thinning by imaging the disintegrated network and remaining partial pore structures post-washing (Fig. 2I).

### 3.2. Design and printing of HEALs

To establish a universal printing protocol for organ or tissue printing using OPEN, it is necessary to first determine a compatible bioink. We selected GelMA, a widely adopted photocrosslinkable collagen-like extracellular matrix protein commonly used in bioprinting (Supplementary Fig. 5). Photocrosslinkable bioink is particularly useful because it does not require specific crosslinking conditions or the presence of additional crosslinkers within the bioink [42]. Using GelMA and OPEN, we determined the best means of printing a functional organ with vein structures. Our protocol is optimized for 3D-printed HEALs, due to the need for liver transplant alternatives [43–47]. And liver bioprinting with additional liver architecture using GelMA/OPEN is also believed to greatly facilitate the potential application of bioengineering transplantation. To design a printing path resulting in a liver structure, we adopted Couinaud's human liver segmental anatomy as guidance for hepatic vein design, including the hepatic veins and the main portal vein (Supplementary Figs. 6A and 6B). Thick tissue or organ reconstruction is challenging in conventional printing due to volume restriction and limited mass transfer in the absence of perfused vasculature. To leverage the design freedom provided by embedded printing, we allocated a lattice printing pathway for the liver and a circular printing pathway for the vasculature (Supplementary Fig. 6C). A steric lattice design was used to optimize oxygen and nutrient transport by alternatively depositing horizontal and vertical filaments for each single layer [48]. Steric lattice design also ensures equivalent filament-to-filament distance within the print, which is not possible in conventional printing due to gravitational restriction. One can also control printing parameters such as grid layout, grid density, and strand width to tailor the resulting construct for each tissue (Supplementary Fig. 7). Combining with endothelial cell-laden tubular vein constructs, we printed an artificial liver model with the major vein systems for further biomedical assessments.

### 3.3. Biocompatibility and activity of mouse hepatocytes in HEAL constructs

In order to promote liver functions in cells within HEAL constructs, printed PMHs were cultivated with specific culture medium in order to assemble into hepatospheroids [20] (Fig. 3A). We first cultured HEAL *in vitro* for 21 days to investigate the viability of PMHs. High viability (>90 %) after 10 days and relatively high viability (>80 %) after 21 days *in vitro* were observed (Fig. 3B and Supplementary Fig. 8). To determine cell activity in the printed constructs, we analyzed hepatospheroid morphology and hepatic marker protein expression using immunofluorescence staining. Hepatorgnoids exhibited high ALB and AAT fluorescence after 10 days cultivation (Fig. 3C and D and Supplementary Fig. 9), indicating liver function. Encapsulated PMHs self-organized into spheroidal constructs throughout the HEAL print and acquired the characteristic polygonal shape of functional hepatocytes [49]. Hepatospheroids also expressed the following hepatic metabolism marker proteins without further induction: GST, MRP2, and CYP enzymes (Supplementary Fig. 10).

Functionally, hepatospheroids exhibited hallmark abilities of mature hepatocytes. The cells imported Dil-ac-LDL into the cytoplasm and stained positive by PAS staining, demonstrating glycogen storage ability (Fig. 3E and F). Furthermore, the ICG uptake and release assay revealed the cells' functional status (Fig. 3G). Additionally, the presence of intermediate layers within a 10-day-old HEAL, showed functional protein secretion prior to transplantation. (Supplementary Fig. 11).

To further support the notion that hepatospheroids in HEAL exhibit hepatic functions, in addition to analyzing morphology and functional activity, we accessed fundamental liver-specific gene expression using qRT-PCR. We hypothesized that PMHs in HEAL benefit from steric lattice design, since oxygen and nutrients can freely diffuse throughout the construct due to assured uniform filament-to-filament distance [50]. To this end, we analyzed two groups of PMHs: (1) PMHs in 2D culture and

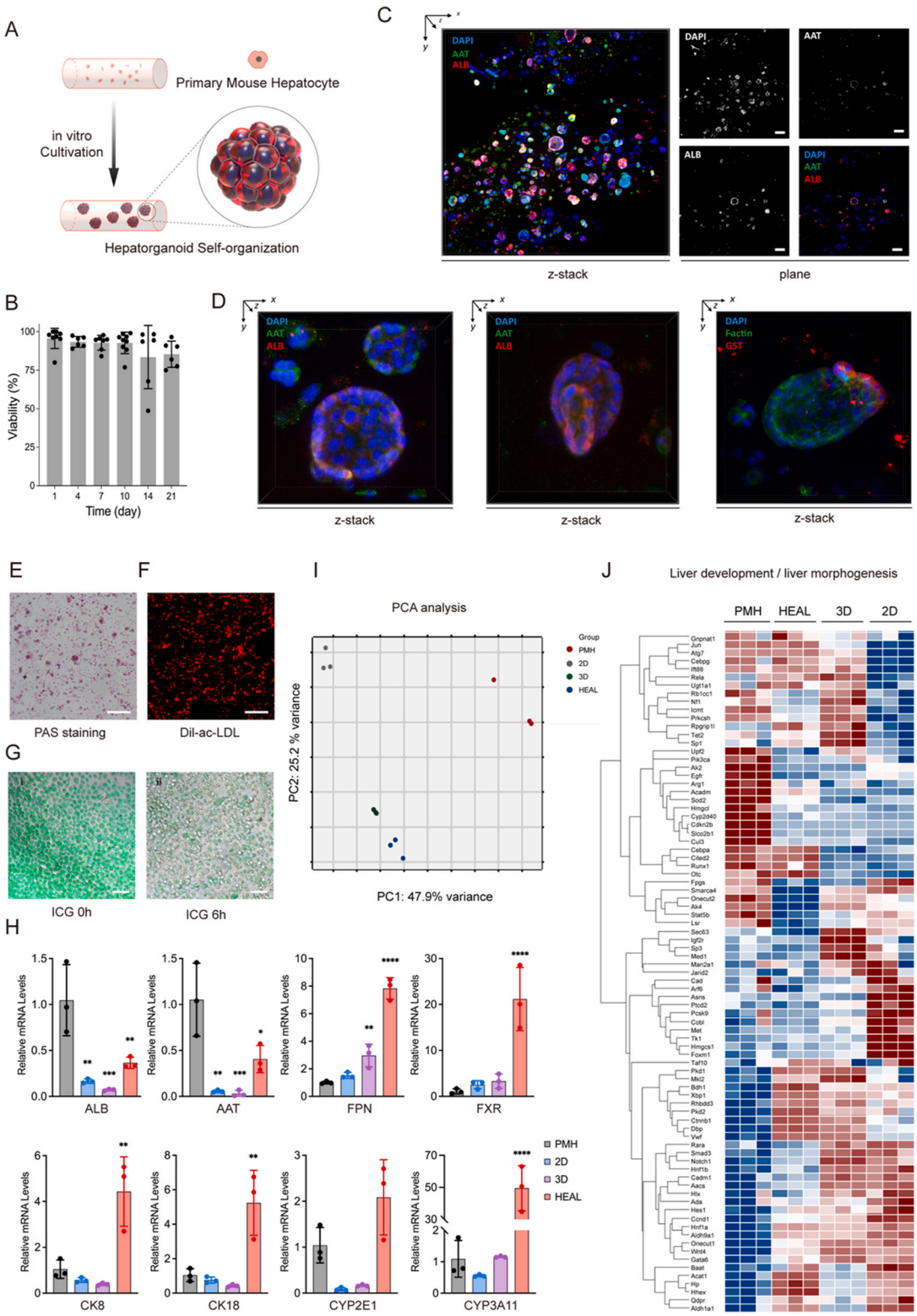


**Fig. 3. In vitro characterizations of the encapsulated hepatospheroids.** (A) Self-organization of PMHs into hepatospheroids *in vitro*. (B) Live/dead assay of printed PMHs demonstrates a good viability rate (>80 %) over 21 days of culturing. n ≥ 6 for biological replicates. (C) Confocal (z stack, left) and plane (right) images of mature hepatospheroids. Scale bar = 100 μm. (D) Confocal z stack images of hepatospheroids in GelMA bioink. Left and middle: AAT (green), ALB (red) and DAPI (blue). Right: GST (red), F-actin (green) and DAPI (blue). Scale bar = 20 μm. (E) Glycogen storage illustrated by PAS staining. Scale bar, 200 μm. (F) Low density lipoprotein uptake determined by Dil-ac-LDL fluorescent staining. Scale bar, 100 μm. (G) ICG uptake and release within 6hr. Scale bar = 100 μm. (H) Expression of hepatic marker gene detected by qPCR analysis over 10 days of culturing. Data are presented as mean ± SD. Statistical significance was determined using one-way ANOVA. $^{*}P < 0.05$, $^{**}P < 0.01$, $^{***}P < 0.01$, $^{****}P < 0.005$, ; n = 3 biological replicates. (I) Principal components analysis of the 12 samples. Each dot represents an individual sample. K-means clustering is denoted by the color of the dots (k = 4). (J) Heatmap showing the hierarchical clustering of the liver development/liver morphogenesis-associated gene expression in PMHs (n = 3), HEAL (n = 3), 2D (n = 3) and 3D (n = 3).

(2) PMHs 3D cultured in bulk or HEAL matrix. Gene expression patterns from freshly isolated PMHs was harnessed as the control group of functional hepatocyte gene expression. For cells cultured in HEAL for 10 days, the expression level of essential hepatocyte specific genes, such as Alb and Aat, was 40 % of that of freshly isolated PMHs. Other hepatic marker genes, including Ferroportin (Fpn), Cytokeratin 8 (Krt8) and Cytokeratin 18 (Krt18), were expressed in significantly higher levels within HEAL constructs than those in 2D, bulk 3D, and even the PMHs control group. Similar results were observed for cytochrome P450, family 2, subfamily e, polypeptide 1 (Cyp2e1) and cytochrome P450, family 3, subfamily a, polypeptide 11 (Cyp3a11, human CYP3A4 equivalent) expression, indicating cytochrome P450 metabolism in HEAL constructs. Collectively, these results suggest that hepatospheroids in HEAL exhibited improved liver function compared to those in 2D and 3D bulk culture conditions (Fig. 3H). To systematically assess the gene expression profiles of hepatospheroids in HEAL, and interrogate

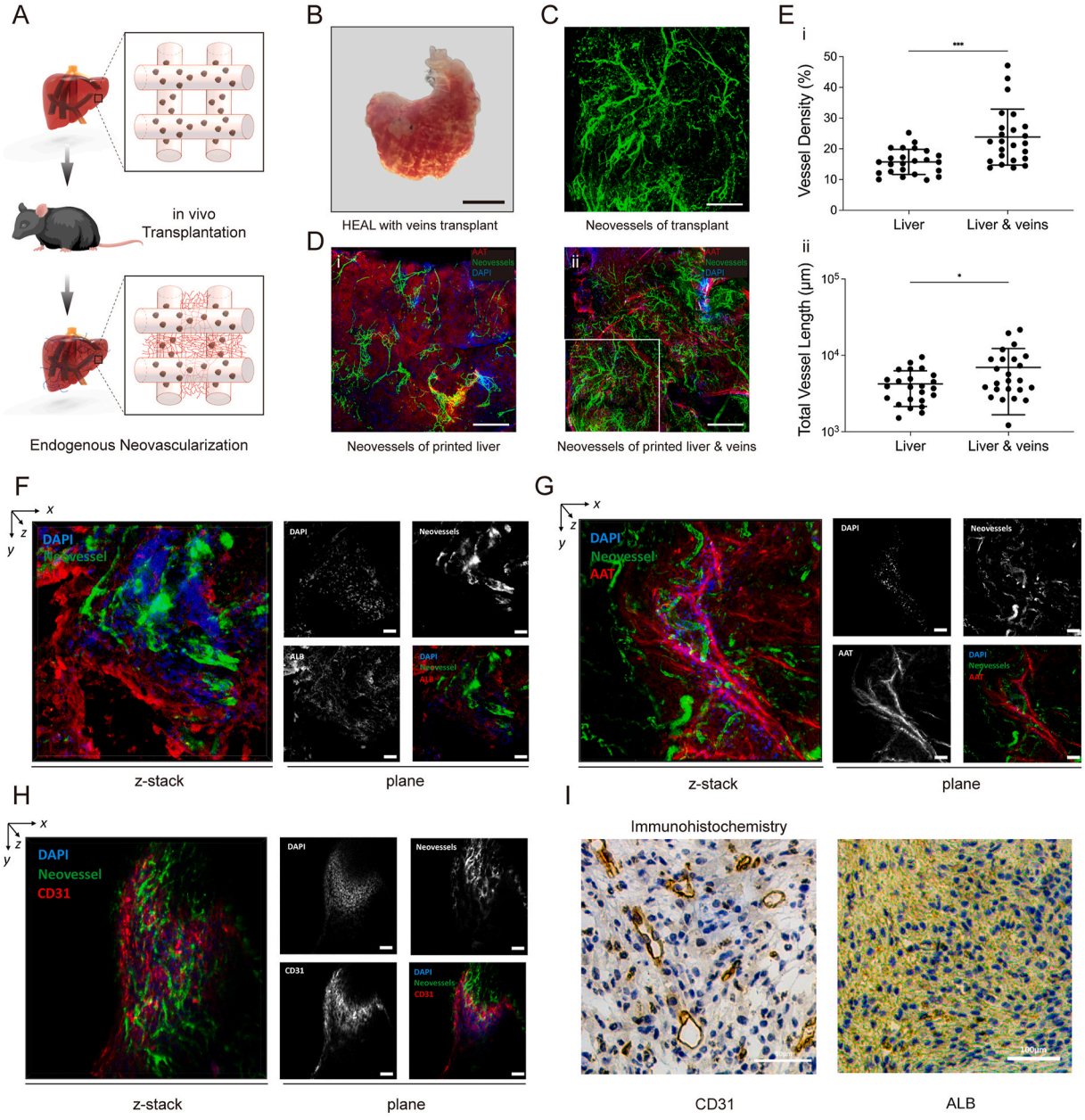


**Fig. 4. In vivo neovascularization of the HEAL transplants with or without vein structures.** (A) Schematic diagram of endogenous neovascularization through the reserved interspace between hepatospheroid-laden strands. (B) Bright field image of vascularized HEAL after 14 days transplantation, showing the angiogenesis over the free space of printed latticed construct. Scale bar, 20 mm. (C) Fluorescent dextran infusion through tail vein injection, displaying functional neovessels within the transplant. Scale bar, 200 μm. (D) Fluorescent images of neovessels on AAT positive transplant parts, showing vascularization from the host into printed HEAL transplants. (i) Neovascularization of HEAL without veins. (ii) Neovascularization of HEAL with veins. Scale bar, 500 μm. (E) Quantification of vascular density and total vessel length of HEAL with or without veins, respectively. (i) HEAL with veins demonstrate 10 % increase in average vessel density compared to HEAL printing alone. (ii) Total vessels length of HEAL with veins increases around 1.6-fold compared to HEAL printing alone. Data are presented as mean ± SD. Statistical significance was determined using an unpaired two-tailed *t*-test. $^{*}P < 0.05$, $^{***}P < 0.01$; n = 6 biological replicates. (F–G) Confocal (z stack, left) and plane (right) images of neovessels on top of hepatic marker (ALB and AAT) positive transplant components. ALB or AAT (red), Neovessels (green) and DAPI (blue). Scale bar = 200 μm. (H) Confocal (z stack, left) and plane (right) images of neovessels on top of vascular marker CD31 positive transplant components. CD31 (red), Neovessels (green) and DAPI (blue). Scale bar = 200 μm. (I) CD31 and ALB immunohistochemical staining of transplant slides, confirming the maintained hepatic function and significant neovascularization within transplanted HEAL.

the difference between HEAL and 2D, 3D cultures, we performed bulk mRNA sequencing. Fig. 3J shows the heatmap of 83 hepatic function-associated genes (liver development/GO:0001889 and liver morphogenesis/GO:0072576). The hepatic gene expression pattern of HEAL closely resembled that of freshly isolated PMHs (Fig. 3I and J). Notably, expression of key hepatocyte transcription factors, such as Jun, Cebpa, Cited2, Runx1 and Otc, was high in both freshly isolated PMHs and HEAL, but not in 2D or 3D cultured PMHs. Additionally, we performed differential gene analysis between PMHs, HEAL and 2D group, and from the analysis we generated 6 clusters with similar expression patterns. Intriguingly, protein-protein interaction (PPI) analysis of the DEGs reveals multiple hepatic and ribosomal genes that are downregulated in 2D but restored to normal level in HEAL condition (as shown in cluster 4, Supplementary Fig. 12). Together, these findings suggest that the translational control and nonalcoholic fatty liver disease (NAFLD)-associated route may have allowed hepatospheroids in HEAL to maintain liver function (Supplementary Fig. 12).

### 3.4. Neovascularization of HEAL constructs in vivo

Since *in vitro* mini-liver reconstruction via HEAL constructs exhibits liver structure and function, we next assessed construct performance *in vivo* to better understand its potential for liver transplantation. HEALs were cultivated *in vitro* for 2 weeks, transplanted into a mouse, and left for another 2 weeks *in vivo* (Fig. 4A). Endogenous neovascularization is crucial for hepatocyte spheroid maintenance *in vivo*, as vasculature is required for oxygen and nutrients delivery and thus cell function and survival [51,52]. We hypothesized that the reserved interspaces between layers and strands from the lattice design might assist angiogenesis *in vivo* compared to conventional prints. However, angiogenesis in HEALs alone did not significantly differ from angiogenesis in conventional 3D-printed liver constructs (Supplementary Fig. 13). To address this issue, we modified the HEAL print design to include the hepatic vein and portal vein, and incorporated C166 cells into the vein prints as cellular building blocks (Fig. 4B and Supplementary Fig. 14). Vascular endothelial growth factor (VEGF) was applied to C166-laden bioink to promote endothelial cell proliferation.

The fully realized HEALs displayed a 10 % increase in average neovessel density and a 60 % increase in total vessel length, suggesting enhanced angiogenesis (Fig. 4C, D, 4E and Supplementary Fig. 15). This improvement is likely due to the introduction of printed endothelial cells, and the VEGF within printed veins [53,54]. While spatial lattice design alone is insufficient to enhance neovascularization, the combination of endotheliocyte-laden veins and spatial lattice design may work synergistically to promote angiogenesis *in vivo*. The superimposition of microscopy images featuring positive ALB, AAT staining, along with fluorescent-labeled vascular networks, provides evidence for the coexistence of functional hepatocytes and neovessels, indicating that the integrated approach effectively supports both liver cell function and vascular growth within the 3D-printed HEAL (Fig. 4F and G).

Noticeably, we observed endogenous neovascularization on the outer surface of the printed veins. Concurrently, the printed veins exhibited a lining of embedded cells, suggesting that the embedded endothelial cells had formed a confluent layer (Fig. 4H). This observation implied that neovessels extensively permeated the interior of the transplanted HEAL prints, given that the printed veins were situated at the center of the HEAL construct (Supplementary Fig. 14). As the printed endothelial cell-laden veins served as a nidus for angiogenesis after transplantation, the neovessels were able to gradually infiltrate the interior of the transplanted HEAL, thereby enhancing nutrient and oxygen delivery to the implanted tissue [55]. This integration process ultimately supported the implant's functionality and survival, which was a critical aspect for the successful transplantation of bioengineered tissues and organs [56]. Moreover, the employment of the spatial lattice design, combined with the incorporation of endotheliocyte-laden veins, may enhance angiogenesis *in vivo*, ultimately leading to a more effective performance of the HEAL construct. We utilized IHC staining to visualize widespread vascularization, that positive CD31 staining displayed endogenous angiogenesis *in vivo* (Fig. 4I). In addition, IHC staining revealed that HEALs preserved excellent hepatic function following transplantation for 2 weeks (Fig. 4I, Supplementary Fig. 16).

## 4. Discussion

3D bioprinting is an efficient method to create models with biomimetic microenvironments pivotal for drug screening and tissue regeneration [57]. Over the past decade, there has been a notable increase in the studies of implantation and functional evaluation of bioprinted constructs using pre–clinical models [21,58,59]. However, clinical translation of conventional bioprinted products is hindered due to the challenges in fabricating large–sized, hollow tubular constructs and entire organs like heart and kidney. This is because the existing bioprinters fail to replicate the native microvasculature and are prone to cause collapse in larger constructs owing to gravitational forces [60]. Embedded bioprinting is an emerging solution to challenge as this novel gel-in-a-gel approach uses mechanically weak or low-viscosity bioinks to produce large and complex 3D constructs by mitigating the gravitational forces [60]. The utilization of support bath facilitates the printing of several complex structures, including bone [61], and heart [62]with enhanced shape fidelity.

Liver is a vital and intricate organ with human body, with multiple functions of synthesis and secretion, drug metabolism, blood coagulation, and immunity. While liver transplantation serves as a practical solution for end-stage liver disease, its efficacy is limited by donor scarcity and immunological rejection. Liver tissue regenerative engineering has emerged as a promising strategy for the potential replacement of liver donors [63]. Prior studies of liver bioprinting predominantly relied on extrusion-based 3D bioprinting techniques, employing gelatin or alginate as bioinks and producing grid-shaped constructs constrained to small size, typically 1cm × 1 cm and 4 layers thick [21,64,65]. The realization of large-sized organ-level liver bioprinting with vasculature remains elusive. In the light of this limitations, we propose exploring the feasibility of using the innovative support medium OPEN to print mini-liver with vein structures and assess their hepatic functions and angiogenic potential.

We firstly customized a biomanufacturing protocol based on the combination of OPEN and GelMA, a one-time forming extracellular matrix (Fig. 1B and C). We then designed printing paths based on segmental liver anatomy, and printed these structures with living cells embedded in the GelMA ink (Fig. 1D). Representative PMHs and C166 cells were used as the encapsulated cellular building blocks to reconstruct biologically functional HEALs with vein structures *in vitro* (Fig. 1E). Within HEAL, PMHs self-organized into hepatocyte spheroids *in vitro,* expressed multiple hepatic markers and exhibited improved liver function and hepatic gene expression compared to conventional 2D or 3D bulk cultivation conditions (Fig. 3). We then transplanted the bioactive HEALs into mice, and left them *in vivo* for two weeks (Fig. 2A). The hepato-spheroid encapsulated transplants promoted endogenous neovascularization and maintained marker protein expression from mature hepato-spheroids *in vivo* (Fig. 2B–H). HEAL transplants with endothelial cell-laden veins promoted *in vivo* neovascularization compared to HEALs without veins and conventional grid prints (Fig. 2E). Hence, our research team stands as pioneers in employing embedded printing techniques for liver architecture. We have effectively demonstrated that OPEN, as a novel support medium, enables the embedded bioprinting of 3D-HEAL with vein structures, exhibiting satisfactory hepatic functions *in vitro* and angiogenic potential *in vivo* post-transplantation.

Despite our research achievements in 3D embedded bioprinting for constructing liver tissue, we are still acutely aware that the structure and function of HEAL with vein structures are still far from real liver. The liver's complexity encompasses a highly intricate anatomical framework

and a diverse array of physiological functions, with hepatic lobules serving the building block. These lobules consist of a portal triad, hepatocytes arranged in linear cords between a capillary network, and a central vein. Apart from the hepatocytes, liver harbors an intricate network of ducts, including the Glisson system, the hepatic venous system and the biliary system. Thus, while reproduction of well-functioning hepato-spheroids and vein structures is imperative, replicating arterial structure and biliary ducts is equally essential yet challenging. Our investigation also had limitations in exploring the interactions between hepatic and endothelial cells, both *in vivo* and *in vitro*. Additionally, we did not thoroughly investigate how modifications in biomaterial properties and cellular spatial arrangements might impact these interactions. Moreover, at the cellular level, beyond hepatocytes and endothelial cells, cholangiocytes, stellate cells, and various immune cells such as Kupffer, are indispensable to achieve the full function of liver. We anticipate further advancements in multicellular liver bioprinting, which could better mimic hepatic microarchitecture and functions. The realization of such goal depends on further improvements in bioprinting technology, including multi-nozzle linkage printing, and the ongoing development of bioinks and multi-cell co-culture system capable of supporting the growth and interaction of multiple cell types.

## 5. Conclusion

In summary, we developed a bulk gel support medium called OPEN, combined this medium with compatible bioink, and created HEAL constructs which retain liver function *in vitro* and promote neovascularization *in vivo*. The facile preparation, straightforward removal method, and the ease of combining OPEN with different bioinks and crosslinking methods make OPEN a useful tool for 3D bioprinting of tissues or organs. With the ongoing advancements in reprogramming and differentiation of human cells, our platform offers a ready-made route to design printing structures with a wide range of cell types in order to recapitulate target tissues or organs with high structural and functional similarities. We envision that our protocol will pave the way for personalized regenerative medicine that could one day serve as transplantable substitutes being used in organ function replacement surgery.

## Funding

This study was supported by the Ministry of Science and Technology of China (MOST; 2019YFA0801501), CAMS Innovation Fund for Medical Sciences (2021-I2M-1–058, 2022-I2M-2–003, 2021-RC310-004), Tianjin Natural Science Foundation for Distinguished Young Scholars (21JCJQJC00030), CAMS start-up grants (2021-RC310-004, 2020-RC310-007), National High Level Hospital Clinical Research Funding (2022-PUMCH-B-034), and National Natural Science Foundation of China (31970687, 32271470), Beijing Municipal Natural Science Foundation (No. 7212077), and China Postdoctoral Science Foundation (No. 2022TQ0042).

## CRediT authorship contribution statement

**Zhuoran Jiang:** Conceptualization, Investigation, Methodology, Formal Analysis, Visualization, Writing – original draft, Writing – review & editing. **Bao Jin:** Investigation, Funding acquisition, Methodology, Writing – review & editing. **Zhu Liang:** Investigation, Methodology, Formal Analysis, Visualization, Writing – original draft, Writing – review & editing. **Yinhan Wang:** Investigation, Formal Analysis, Visualization, Writing – original draft, Writing – review & editing. **Shuai Ren:** Investigation, Formal Analysis, Writing – review & editing. **Yongfa Huang:** Investigation, Resources, Writing – review & editing. **Changcan Li:** Investigation, Resources, Writing – review & editing. **Hang Sun:** Investigation, Resources, Writing – review & editing. **Yunzhu Li:** Resources, Writing – review & editing. **Li Liu:** Formal Analysis, Writing – review & editing. **Nianlin Li:** Formal Analysis, Writing – review & editing. **Jinzhuo Wang:** Formal Analysis, Writing – review & editing. **Zhanfeng Cui:** Conceptualization, Writing – review & editing. **Pengyu Huang:** Conceptualization, Funding acquisition, Project administration, Supervision, Writing – review & editing. **Huayu Yang:** Conceptualization, Formal Analysis, Funding acquisition, Project administration, Supervision, Writing – review & editing. **Yilei Mao:** Conceptualization, Formal Analysis, Funding acquisition, Project administration, Supervision, Writing – review & editing. **Hua Ye:** Conceptualization, Project administration, Supervision, Writing – review & editing.

## Declaration of competing interest

The authors declare that they have no known competing financial interests or personal relationships that could have appeared to influence the work reported in this paper.

## Data availability

The authors are unable or have chosen not to specify which data has been used.

## Acknowledgement

ZJ acknowledge the Jardine Foundation for financial support. We thank Dr. Casey Adam for helpful suggestions in preparation of the manuscript.

## Appendix A. Supplementary data

Supplementary data to this article can be found online at https://doi.org/10.1016/j.biomaterials.2024.122681.

## References

[1] L. Moroni, J.A. Burdick, C. Highley, S.J. Lee, Y. Morimoto, S. Takeuchi, J.J. Yoo, Biofabrication strategies for 3D in vitro models and regenerative medicine, Nat. Rev. Mater. 3 (5) (2018) 21–37.
[2] S.V. Murphy, A. Atala, 3D bioprinting of tissues and organs, Nat. Biotechnol. 32 (8) (2014) 773–785.
[3] R. Levato, T. Jungst, R.G. Scheuring, T. Blunk, J. Groll, J. Malda, From shape to function: the next step in bioprinting, Adv. Mater. 32 (12) (2020) e1906423.
[4] Y. Gu, A. Forget, V.P. Shastri, Biobridge: an outlook on translational bioinks for 3D bioprinting, Adv. Sci. 9 (3) (2022) e2103469.
[5] Z. Jiang, O. Erol, D. Chatterjee, W. Xu, N. Hibino, L.H. Romer, S.H. Kang, D. H. Gracias, Direct ink writing of poly(tetrafluoroethylene) (PTFE) with tunable mechanical properties, ACS Appl. Mater. Interfaces 11 (31) (2019) 28289–28295.
[6] J. Jang, H.J. Park, S.W. Kim, H. Kim, J.Y. Park, S.J. Na, H.J. Kim, M.N. Park, S. H. Choi, S.H. Park, S.W. Kim, S.M. Kwon, P.J. Kim, D.W. Cho, 3D printed complex tissue construct using stem cell-laden decellularized extracellular matrix bioinks for cardiac repair, Biomaterials 112 (2017) 264–274.
[7] A. Arslan-Yildiz, R. El Assal, P. Chen, S. Guven, F. Inci, U. Demirci, Towards artificial tissue models: past, present, and future of 3D bioprinting, Biofabrication 8 (1) (2016) 014103.
[8] S. Chawla, S. Midha, A. Sharma, S. Ghosh, Silk-based bioinks for 3D bioprinting, Adv. Healthcare Mater. 7 (8) (2018) e1701204.
[9] I. Donderwinkel, J.C.M. van Hest, N.R. Cameron, Bio-inks for 3D bioprinting: recent advances and future prospects, Polym. Chem. 8 (31) (2017) 4451–4471.
[10] Z. Fu, L. Ouyang, R. Xu, Y. Yang, W. Sun, Responsive biomaterials for 3D bioprinting: a review, Mater. Today 52 (2022) 112–132.
[11] T.J. Hinton, Q. Jallerat, R.N. Palchesko, J.H. Park, M.S. Grodzicki, H.J. Shue, M. H. Ramadan, A.R. Hudson, A.W. Feinberg, Three-dimensional printing of complex biological structures by freeform reversible embedding of suspended hydrogels, Sci. Adv. 1 (9) (2015) e1500758.
[12] T. Bhattacharjee, S.M. Zehnder, K.G. Rowe, S. Jain, R.M. Nixon, W.G. Sawyer, T. E. Angelini, Writing in the granular gel medium, Sci. Adv. 1 (8) (2015) e1500655.
[13] C.S. O'Bryan, T. Bhattacharjee, S. Hart, C.P. Kabb, K.D. Schulze, I. Chilakala, B. S. Sumerlin, W.G. Sawyer, T.E. Angelini, Self-assembled micro-organogels for 3D printing silicone structures, Sci. Adv. 3 (5) (2017) e1602800.
[14] J. Zhao, N. He, A mini-review of embedded 3D printing: supporting media and strategies, J. Mater. Chem. B 8 (46) (2020) 10474–10486.
[15] A. Lee, A.R. Hudson, D.J. Shiwarski, J.W. Tashman, T.J. Hinton, S. Yerneni, J. M. Bliley, P.G. Campbell, A.W. Feinberg, 3D bioprinting of collagen to rebuild components of the human heart, Science 365 (6452) (2019) 482–487.

[16] N. Noor, A. Shapira, R. Edri, I. Gal, L. Wertheim, T. Dvir, 3D printing of personalized thick and perfusable cardiac patches and hearts, Adv. Sci. 6 (11) (2019) 1900344.
[17] J. Laurent, G. Blin, F. Chatelain, V. Vanneaux, A. Fuchs, J. Larghero, M. Théry, Convergence of microengineering and cellular self-organization towards functional tissue manufacturing, Nat. Biomed. Eng. 1 (12) (2017) 939–956.
[18] J. Best, P. Manka, W.K. Syn, L. Dollé, L.A. van Grunsven, A. Canbay, Role of liver progenitors in liver regeneration, Hepatobiliary Surg. Nutr. 4 (1) (2015) 48–58.
[19] J.S. Witowski, J. Coles-Black, T.Z. Zuzak, M. Pędziwiatr, J. Chuen, P. Major, A. Budzyński, 3D printing in liver surgery: a systematic review, Telemed. J. e Health 23 (12) (2017) 943–947.
[20] M. Luo, J. Lai, E. Zhang, Y. Ma, R. He, L. Mao, B. Deng, J. Zhu, Y. Ding, J. Huang, B. Xue, Q. Wang, M. Zhang, P. Huang, Rapid self-assembly mini-livers protect mice against severe hepatectomy-induced liver failure, Adv. Sci. (2024) e2309166.
[21] H. Yang, L. Sun, Y. Pang, D. Hu, H. Xu, S. Mao, W. Peng, Y. Wang, Y. Xu, Y. C. Zheng, S. Du, H. Zhao, T. Chi, X. Lu, X. Sang, S. Zhong, X. Wang, H. Zhang, P. Huang, W. Sun, Y. Mao, Three-dimensional bioprinted hepatorganoids prolong survival of mice with liver failure, Gut 70 (3) (2021) 567–574.
[22] S. Mao, J. He, Y. Zhao, T. Liu, F. Xie, H. Yang, Y. Mao, Y. Pang, W. Sun, Bioprinting of patient-derived in vitro intrahepatic cholangiocarcinoma tumor model: establishment, evaluation and anti-cancer drug testing, Biofabrication 12 (4) (2020) 045014.
[23] F. Xie, L. Sun, Y. Pang, G. Xu, B. Jin, H. Xu, X. Lu, Y. Xu, S. Du, Y. Wang, S. Feng, X. Sang, S. Zhong, X. Wang, W. Sun, H. Zhao, H. Zhang, H. Yang, P. Huang, Y. Mao, Three-dimensional bio-printing of primary human hepatocellular carcinoma for personalized medicine, Biomaterials 265 (2021) 120416.
[24] C. Li, B. Jin, H. Sun, Y. Wang, H. Zhao, X. Sang, H. Yang, Y. Mao, Exploring the function of stromal cells in cholangiocarcinoma by three-dimensional bioprinting immune microenvironment model, Front. Immunol. 13 (2022) 941289.
[25] Y. Jin, A. Compaan, W. Chai, Y. Huang, Functional nanoclay suspension for printing-then-solidification of liquid materials, ACS Appl. Mater. Interfaces 9 (23) (2017) 20057–20066.
[26] A.M. Compaan, K. Song, Y. Huang, Gellan fluid gel as a versatile support bath material for fluid extrusion bioprinting, ACS Appl. Mater. Interfaces 11 (6) (2019) 5714–5726.
[27] Q. Li, Z. Jiang, L. Ma, J. Yin, Z. Gao, L. Shen, H. Yang, Z. Cui, H. Ye, H. Zhou, A versatile embedding medium for freeform bioprinting with multi-crosslinking methods, Biofabrication 14 (3) (2022).
[28] M. Okubo, D. Iohara, M. Anraku, T. Higashi, K. Uekama, F. Hirayama, A thermoresponsive hydrophobically modified hydroxypropylmethylcellulose/cyclodextrin injectable hydrogel for the sustained release of drugs, Int. J. Pharm. 575 (2020) 118845.
[29] W. Wu, A. DeConinck, J.A. Lewis, Omnidirectional printing of 3D microvascular networks, Adv. Mater. 23 (24) (2011) H178–H183.
[30] E.A. Appel, M.W. Tibbitt, M.J. Webber, B.A. Mattix, O. Veiseh, R. Langer, Self-assembled hydrogels utilizing polymer-nanoparticle interactions, Nat. Commun. 6 (2015) 6295.
[31] J.B. da Silva, R.S. Dos Santos, M.B. da Silva, G. Braga, M.T. Cook, M.L. Bruschi, Interaction between mucoadhesive cellulose derivatives and Pluronic F127: investigation on the micelle structure and mucoadhesive performance, Mater. Sci. Eng., C 119 (2021) 111643.
[32] D. Iohara, M. Okubo, M. Anraku, S. Uramatsu, T. Shimamoto, K. Uekama, F. Hirayama, Hydrophobically modified polymer/α-cyclodextrin thermoresponsive hydrogels for use in ocular drug delivery, Mol. Pharm. 14 (8) (2017) 2740–2748.
[33] B. Shriky, A. Kelly, M. Isreb, M. Babenko, N. Mahmoudi, S. Rogers, O. Shebanova, T. Snow, T. Gough, Pluronic F127 thermosensitive injectable smart hydrogels for controlled drug delivery system development, J. Colloid Interface Sci. 565 (2020) 119–130.
[34] B. Alonso-Lerma, L. Barandiaran, L. Ugarte, I. Larraza, A. Reifs, R. Olmos-Juste, N. Barruetabeña, I. Amenabar, R. Hillenbrand, A. Eceiza, R. Perez-Jimenez, High performance crystalline nanocellulose using an ancestral endoglucanase, Communications Materials 1 (1) (2020) 57.
[35] P. Krishnamachari, R. Hashaikeh, M. Tiner, Modified cellulose morphologies and its composites; SEM and TEM analysis, Micron 42 (8) (2011) 751–761.
[36] S.B.S. Ferreira, G. Braga, L. Oliveira É, J.B. da Silva, H.C. Rosseto, L.V. de Castro Hoshino, M.L. Baesso, W. Caetano, C. Murdoch, H.E. Colley, M.L. Bruschi, Design of a nanostructured mucoadhesive system containing curcumin for buccal application: from physicochemical to biological aspects, Beilstein J. Nanotechnol. 10 (2019) 2304–2328.
[37] A.M. Pragatheeswaran, S.B. Chen, Effect of chain length of PEO on the gelation and micellization of the pluronic F127 copolymer aqueous system, Langmuir 29 (31) (2013) 9694–9701.
[38] L.M. Stapleton, A.N. Steele, H. Wang, H. Lopez Hernandez, A.C. Yu, M.J. Paulsen, A.A.A. Smith, G.A. Roth, A.D. Thakore, H.J. Lucian, K.P. Totherow, S.W. Baker, Y. Tada, J.M. Farry, A. Eskandari, C.E. Hironaka, K.J. Jaatinen, K.M. Williams, H. Bergamasco, C. Marschel, B. Chadwick, F. Grady, M. Ma, E.A. Appel, Y.J. Woo, Use of a supramolecular polymeric hydrogel as an effective post-operative pericardial adhesion barrier, Nat. Biomed. Eng. 3 (8) (2019) 611–620.
[39] A. Colly, C. Marquette, E.J. Courtial, Poloxamer/Poly(ethylene glycol) self-healing hydrogel for high-precision freeform reversible embedding of suspended hydrogel, Langmuir 37 (14) (2021) 4154–4162.
[40] O. Boonrat, V. Tantishaiyakul, N. Hirun, S. Rugmai, S. Soontaranon, Structural characterization using SAXS and rheological behaviors of pluronic F127 and methylcellulose blends, Polym. Bull. 78 (2020) 1175–1187.
[41] Z. Wei, J.H. Yang, J. Zhou, F. Xu, M. Zrínyi, P.H. Dussault, Y. Osada, Y.M. Chen, Self-healing gels based on constitutional dynamic chemistry and their potential applications, Chem. Soc. Rev. 43 (23) (2014) 8114–8131.
[42] L. Sun, L. Hui, Progress in human liver organoids, J. Mol. Cell Biol. 12 (8) (2020) 607–617.
[43] C. Li, Z. Jiang, H. Yang, Advances in 3D bioprinting technology for liver regeneration, Hepatobiliary Surg. Nutr. 11 (6) (2022) 917–919.
[44] J. Zhang, H. Yang, H. Yang, Highlights of constructing liver-relevant in vitro models with 3D bioprinting, Hepatobiliary Surg. Nutr. 11 (6) (2022) 896–898.
[45] G. Xu, C.H. Jiang, T. Lv, J.L. Song, Y.J. Zhou, J. Yang, L. Jiang, L.N. Yan, K. Luo, J. Y. Yang, Developing a new nomogram to predict early allograft dysfunction after liver transplantation: a nudge in the right direction, Hepatobiliary Surg. Nutr. 11 (3) (2022) 462–466.
[46] J.H. Koh, D.J.H. Tan, Y. Ong, W.H. Lim, C.H. Ng, P.W.L. Tay, J.N. Yong, M. D. Muthiah, E.X. Tan, N.Q. Pang, B.K. Kim, N. Syn, A. Kow, B.K.P. Goh, D. Q. Huang, Liver resection versus liver transplantation for hepatocellular carcinoma within Milan criteria: a meta-analysis of 18,421 patients, Hepatobiliary Surg. Nutr. 11 (1) (2022) 78–93.
[47] P. Gavrilidis, E. Hidalgo, Alternatives to left lateral sector in paediatric liver transplantation-a systematic review on monosegmental and reduced grafts, Hepatobiliary Surg. Nutr. 11 (4) (2022) 567–576.
[48] H.W. Kang, S.J. Lee, I.K. Ko, C. Kengla, J.J. Yoo, A. Atala, A 3D bioprinting system to produce human-scale tissue constructs with structural integrity, Nat. Biotechnol. 34 (3) (2016) 312–319.
[49] W. Zhang, W. Ye, Y. Yan, Advances in photocrosslinkable materials for 3D bioprinting, Adv. Eng. Mater. 24 (1) (2022) 2100663.
[50] Y. He, F. Yang, H. Zhao, Q. Gao, B. Xia, J. Fu, Research on the printability of hydrogels in 3D bioprinting, Sci. Rep. 6 (2016) 29977.
[51] S.P. Harrison, R. Siller, Y. Tanaka, M.E. Chollet, M.E. de la Morena-Barrio, Y. Xiang, B. Patterson, E. Andersen, C. Bravo-Pérez, H. Kempf, K.S. Åsrud, O. Lunov, A. Dejneka, M.C. Mowinckel, B. Stavik, P.M. Sandset, E. Melum, S. Baumgarten, F. Bonanini, D. Kurek, S. Mathapati, R. Almaas, K. Sharma, S. R. Wilson, F.S. Skottvoll, I.C. Boger, I.L. Bogen, T.A. Nyman, J.J. Wu, A. Bezrouk, D. Cizkova, J. Corral, J. Mokry, R. Zweigerdt, I.H. Park, G.J. Sullivan, Scalable production of tissue-like vascularized liver organoids from human PSCs, Exp. Mol. Med. 55 (9) (2023) 2005–2024.
[52] T. Takebe, R.R. Zhang, H. Koike, M. Kimura, E. Yoshizawa, M. Enomura, N. Koike, K. Sekine, H. Taniguchi, Generation of a vascularized and functional human liver from an iPSC-derived organ bud transplant, Nat. Protoc. 9 (2) (2014) 396–409.
[53] A.A. Szklanny, M. Machour, I. Redenski, V. Chochola, I. Goldfracht, B. Kaplan, M. Epshtein, H. Simaan Yameen, U. Merdler, A. Feinberg, D. Seliktar, N. Korin, J. Jaroš, S. Levenberg, 3D bioprinting of engineered tissue flaps with hierarchical vessel networks (VesselNet) for direct host-to-implant perfusion, Adv. Mater. 33 (42) (2021) e2102661.
[54] D.H. Nguyen, S.C. Stapleton, M.T. Yang, S.S. Cha, C.K. Choi, P.A. Galie, C.S. Chen, Biomimetic model to reconstitute angiogenic sprouting morphogenesis in vitro, Proc. Natl. Acad. Sci. U. S. A. 110 (17) (2013) 6712–6717.
[55] Y. He, Y. Wu, J. Fu, Q. Gao, J. Qiu, Developments of 3D printing microfluidics and applications in chemistry and biology: a review, Electroanalysis 28 (2016) 1658–1678.
[56] I.S. Kinstlinger, J.S. Miller, 3D-printed fluidic networks as vasculature for engineered tissue, Lab Chip 16 (11) (2016) 2025–2043.
[57] S. Maharjan, C. Ma, B. Singh, H. Kang, G. Orive, J. Yao, Y. Shrike Zhang, Advanced 3D imaging and organoid bioprinting for biomedical research and therapeutic applications, Adv. Drug Deliv. Rev. 208 (2024) 115237.
[58] S. Abadpour, E.M. Niemi, L.S. Orrhult, C. Hermanns, R. de Vries, L.P. Nogueira, H. J. Haugen, D. Josefsen, S. Krauss, P. Gatenholm, A. van Apeldoorn, H. Scholz, Adipose-Derived stromal cells preserve pancreatic islet function in a transplantable 3D bioprinted scaffold, Adv. Healthcare Mater. 12 (32) (2023) e2300640.
[59] Y. Liu, Y. Zhang, T. Mei, H. Cao, Y. Hu, W. Jia, J. Wang, Z. Zhang, Z. Wang, W. Le, Z. Liu, hESCs-Derived early vascular cell spheroids for cardiac tissue vascular engineering and myocardial infarction treatment, Adv. Sci. 9 (9) (2022) e2104299.
[60] H. Budharaju, D. Sundaramurthi, S. Sethuraman, Embedded 3D bioprinting - an emerging strategy to fabricate biomimetic & large vascularized tissue constructs, Bioact. Mater. 32 (2024) 356–384.
[61] G. Cidonio, M. Cooke, M. Glinka, J.I. Dawson, L. Grover, R.O.C. Oreffo, Printing bone in a gel: using nanocomposite bioink to print functionalised bone scaffolds, Mater Today Bio 4 (2019) 100028.
[62] Y. Fang, Y. Guo, B. Wu, Z. Liu, M. Ye, Y. Xu, M. Ji, L. Chen, B. Lu, K. Nie, Z. Wang, J. Luo, T. Zhang, W. Sun, Z. Xiong, Expanding embedded 3D bioprinting capability for engineering complex organs with freeform vascular networks, Adv. Mater. 35 (22) (2023) e2205082.
[63] L. Sun, Y. Wang, S. Zhang, H. Yang, Y. Mao, 3D bioprinted liver tissue and disease models: current advances and future perspectives, Biomater. Adv. 152 (2023) 213499.
[64] T. Hiller, J. Berg, L. Elomaa, V. Röhrs, I. Ullah, K. Schaar, A.-C. Dietrich, M.A. Al-Zeer, A. Kurtz, A.C. Hocke, S. Hippenstiel, H. Fechner, M. Weinhart, J. Kurreck, Generation of a 3D liver model comprising human extracellular matrix in an alginate/gelatin-based bioink by extrusion bioprinting for infection and transduction studies, Int. J. Mol. Sci. 19 (10) (2018) 3129.
[65] M. Cuvellier, F. Ezan, H. Oliveira, S. Rose, J.-C. Fricain, S. Langouët, V. Legagneux, G. Baffet, 3D culture of HepaRG cells in GelMa and its application to bioprinting of a multicellular hepatic model, Biomaterials 269 (2021) 120611.

## Abrreviations

*OPEN:* omnidirectional printing embedded network
*PMHs:* Primary mouse hepatocytes
*HEALs:* hepatospheroid-encapsulated-artificial livers